arXiv:cond-mat/0307590v1 [cond-mat.mes-hall] 23 Jul 2003

Phase measurements using Two-Channel Fano Interference in a Semiconductor Quantum Dot

C. Fühner,* U. F. Keyser, and R. J. Haug
Institut für Festkörperphysik, Universität Hannover, Appelstr. 2, 30167 Hannover, Germany

D. Reuter and A. D. Wieck
Lehrstuhl für Angewandte Festkörperphysik, Ruhr-Universität Bochum, 44780 Bochum, Germany

(Dated: February 2, 2008)

We investigate a lateral semiconductor quantum dot with a large number of electrons in the semi-open Fano regime. In transport measurements we observe three stable series of Fano resonances with similar lineshapes. We present a simple model explaining the temperature and V_{SD} dependence of the resonances. The Fano regime allows to investigate phase and coherence of the electronic wave function and astonishingly, we find no signs of decoherence in our system.

PACS numbers: 72.15.Qm, 73.21.La, 73.23.Hk, 73.40.Gk

Transport through semiconductor quantum dots [1] has been studied in a number of different regimes. Each regime is characterized by specific lineshapes of the resonances in linear conductance measurements. In the Coulomb regime at weak tunnel coupling between dot and leads basically Breit-Wigner type resonances are observed [2]. At stronger coupling an increased valley conductance indicates the Kondo regime [3]. Experiments with transparent barriers in the open regime are interpreted in terms of ballistic transport with electrons geometrically reflected within the dot [4]. Here, we explore an intermediate regime, the semi-open Fano regime where a ballistic transport channel coexists with a resonant transport channel from Coulomb blockade.

Fano resonances are a very general characteristic of systems where two transmission channels interfere, a resonant and a non-resonant one (Fig. 1(a)). Depending on the relative phase and amplitude of the two channels they exhibit a wide range of lineshapes parameterized by the asymmetry parameter q (Fig. 1(b)). The analytical expression for Fano resonances is [5]:

$$f_{Fano}(\tilde{\varepsilon}) = \frac{(\tilde{\varepsilon}+q)^2}{\tilde{\varepsilon}^2+1} \qquad (1)$$

with $\tilde{\varepsilon} = (\varepsilon - \varepsilon_0)/(\hbar\Gamma/2)$ the detuning from the resonance at energy ε_0 and normalized to the width Γ of the resonance. As shown in Fig. 1(b), we get Breit-Wigner type peaks for $q \to \infty$, dips for $q = 0$, and asymmetric lineshapes in between as shown for $q = 1$. Negative parameters q lead to lineshapes mirrored at the ordinate, i. e. $\tilde{\varepsilon} \to -\tilde{\varepsilon}$.

Fano theory was initially developed in the context of electron-atom scattering [5] but later applied to a large number of other experiments, ranging from electron-neutron scattering [6] to atomic photoionization [7]. More recent observations of Fano resonances in electronic transport experiments include crossed multiwall carbon nanotubes [8], scanning tunneling microscopy of single adatoms on a metallic surface [9] and transport studies of man-made semiconductor nanostructures [10]. Kobayashi and coworkers observed Fano resonances in an Aharonov-Bohm ring with a quantum dot embedded in one arm [11]. The resonant channel in their system stems from Coulomb blockade in the quantum dot, and the non-resonant channel originates from the continuous spectrum of the other arm.

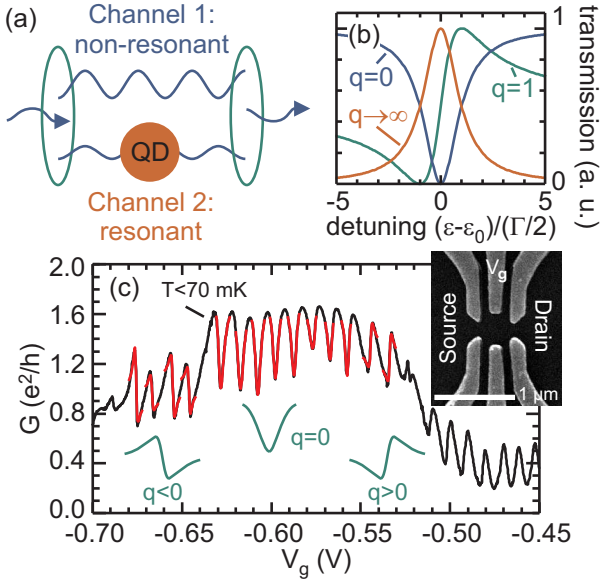

FIG. 1: (a) Model system for Fano resonances. An incident wave function interferes after transmission through two channels, a resonant and a non-resonant one. Here, the resonant channel is formed by a quantum dot (QD). (b) Fano transmission lineshapes parameterized by q. (c) Linear conductance G of our quantum dot versus plunger gate voltage V_g in the semi-open Fano regime exhibiting three regimes with $q < 0$, $q = 0$, and $q > 0$. Fits to the individual resonances are shown in red. Inset: SEM picture of the sample.

In contrast, in pure quantum dot experiments in the semi-open regime the dot itself can be the interferometer. There is no spatial separation between the two transport channels. The resonant transmission mechanism is the same as known from Coulomb blockade. An additional non-resonant transmission channel comes into existence when the time needed to traverse the dot via a direct trajectory, $\Delta t \sim l/v_F$, is small enough (l is the length of the path and v_F the Fermi velocity). Then by the time-energy uncertainty principle with the Coulomb charging

energy U, $\Delta t \cdot U \geq h$, the transmission via the direct path is no longer forbidden by Coulomb blockade. So far, there have been only few experimental studies on quantum dots in the semi-open regime [12, 13]. However, these experiments have generated great theoretical interest [14, 15, 16, 17]. They are sensitive tools to gain information on the phase of transmitted electrons inaccessible in other regimes [18, 19]. It was even suggested to use Fano resonances as a probe of phase coherence in quantum dots.

In this paper, we study a quantum dot in the semi-open Fano regime in low-temperature transport measurements. We extract quantitative information of the two interfering channels including phase. Decoherence is studied by application of finite temperature and source-drain voltage.

We fabricated our sample from a high-mobility GaAs/AlGaAs two-dimensional electron system (2DES) with an electron density $n = 3.7 \cdot 10^{15}$ m^{-2} and a mobility $\mu = 130$ m^2/Vs. Cr/Au split-gates were patterned by electron beam lithography (Fig. 1(c), inset). We apply negative gate voltages to form a quantum dot tunnel coupled to 2DES leads. The plunger gate voltage V_g controls the dot energy levels and – due to spatial proximity to the tunnel barriers – to some extent also influences the coupling of the dot to the leads. We use a standard lock-in technique for differential conductance measurements in a ^{3}He-^{4}He dilution refrigerator with an electronic base temperature less than 70 mK.

We can tune our quantum dot from the closed Coulomb regime to the semi-open Fano regime. Linear conductance measurements in the Fano regime are shown in Fig. 1(c). We clearly observe Fano anti-resonances and asymmetric resonances instead of Breit-Wigner type peaks known from Coulomb blockade. We find three groups of resonances with similar lineshapes corresponding to asymmetry parameters $q < 0$, $q = 0$, and $q > 0$ in the gate voltage range from $V_g = -0.68$ V to $V_g = -0.52$ V. This is different from the continuous evolution of lineshapes in multi-level interference experiments [20]. For $V_g > -0.52$ V the Breit-Wigner lineshape is restored. In the Fano regions, the background conductance is high ($\sim 1 - 2\ e^2/h$) similar to the open regime.

To fit the measured Fano resonances (red curves in Fig. 1(c)), we use eq. 1 with an additional prefactor and offset,

$$f_{exp}(V_g) = A_{exp} \cdot [f_{Fano}(\tilde{\varepsilon}(V_g)) - 1] + B_{exp}. \qquad (2)$$

A_{exp} and B_{exp} account for a reduced transmission amplitude of the two interfering channels, e. g. due to backscattering in one channel, and for an incoherent contribution to the total conductance. The fit parameters A_{exp}, B_{exp} and q are plotted in Fig. 2(a)–(c). The evolution of the parameters exhibits clear steps at the positions marked by the vertical grey lines. The parameters are nearly constant within one group of resonances but change in between.

This switching is further investigated in Fig. 2(d) where we have analyzed the spacing ΔV_g of the resonances in gate voltage. The spacing is nearly constant within any group of resonances but shows increased values at the switching points of the fit parameters. In the two-channel model (Fig. 1(a)), the positions of the Fano resonances are determined by the V_g positions of the Coulomb resonances in the resonant channel. In a large dot like ours, the spacing of Coulomb peaks is dominated by the charging energy U which is large compared to the single-particle energy level spacing ΔE_i, $U > \Delta E_i$. Clear deviations from a constant peak spacing are thus attributed to greater redistributions of the charge on the dot. These redistributions influence the non-resonant transmission channel which also traverses the dot. Consequently, the interference of both channels and hence the Fano lineshape is altered. Within the groups of constantly spaced and similarly shaped Fano resonances, the transmission of the non-resonant channel is constant.

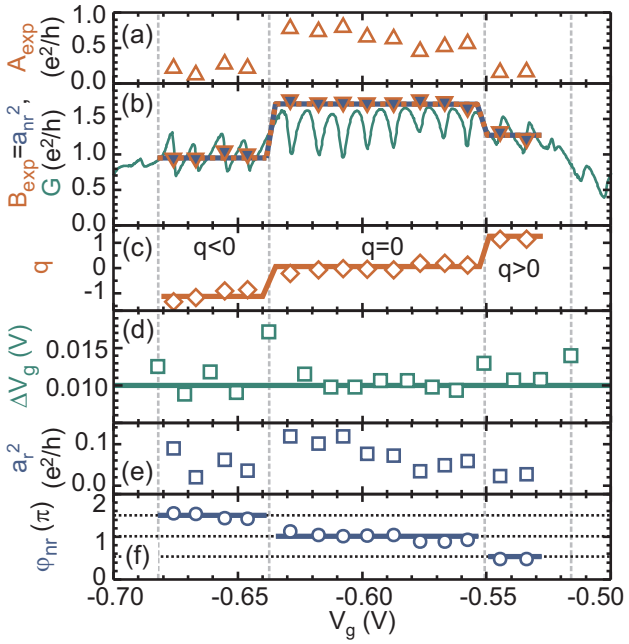

FIG. 2: (a)–(c) Parameters A_{exp}, B_{exp}, and q for fits of individual Fano resonances from Fig. 1(c) to eq. 2 (red). The original linear conductance data is also shown in (b) for reference (green). The vertical lines separate the three groups of similar Fano resonances, the others are guides to the eye. (d) The resonance-to-resonance spacing ΔV_g (squares) is nearly constant as highlighted by the red line. Exceptions coincide with changes in q at the vertical grey lines. (b),(d),(e) show the extracted parameters a_{nr}^2, a_r^2, and φ_{nr} of the two-channel model (blue).

For a quantitative understanding of the Fano resonances, we investigate the model of two interfering channels in more detail: In the non-resonant conductance channel, the electronic wave function evolves like a plane wave. After traversing the channel its amplitude is a_{nr} and its phase is φ_{nr}. Compared to the width of a resonance, the energy dependence of a_{nr} and φ_{nr} is negligible. Thus the complex transmission of the channel is:

$$t_{nr} = a_{nr} \cdot \exp(i\varphi_{nr}). \qquad (3)$$

t_{nr} is modified in charge reconfigurations on the dot but otherwise constant as discussed above.

To model the complex transmission of the resonant channel, we consider a Coulomb resonance at zero temperature ($T = 0$). According to experiments by Schuster *et al.* [21] we use the Breit-Wigner formula with a normalized detuning $\tilde{\varepsilon}$ from resonance and with an amplitude a_r:

$$t_r(\tilde{\varepsilon}) = a_r \cdot \frac{i}{\tilde{\varepsilon} + i} \tag{4}$$

The transmission probability $T_r(\tilde{\varepsilon}) = |t_r(\tilde{\varepsilon})|^2 = a_r^2/(\tilde{\varepsilon}^2 + 1)$ (i. e. the conductance) of this channel yields the well-known Breit-Wigner peaks. The total transmission amplitude

$$T_{tot}(\tilde{\varepsilon}) = |t_{nr} + t_r(\tilde{\varepsilon})|^2. \tag{5}$$

describes the conductance of the complete Fano system from Fig. 1(a) including interference. The comparison of equations 2 and 5 allows to map the phenomenological constants (A_{exp}, B_{exp}, q) determined from the fit to the more physical parameters $(a_{nr}, a_r, \varphi_n r)$. It is easily shown that $a_{nr}^2 = B_{exp}$. The other expressions are more complex due to trigonometric functions.

The transformation of the experimental and phenomenological data from Fig. 2 is shown in the same figure in blue. The non-resonant transmission amplitude a_{nr} and phase φ_{nr} as functions of gate voltage reflect the switching in the non-resonant channel. Phase differences of $\Delta\varphi_{nr} = \pi/2$ correspond to a length difference of at least $\Delta\varphi_{nr}/k_F = 10$ nm (k_F is the Fermi wavevector) between non-resonant channels for different charge configurations. The transmission amplitude a_{nr} varies between 1.0 and 1.7 e^2/h. It thus can be explained by a one-dimensional spin-degenerate channel with its conductance of 2 e^2/h slightly reduced due to backscattering. The backscattering is modified at the steps. In contrast the resonant channel's amplitude a_r^2 exhibits an unsystematic modulation which is well known from Coulomb blockade and is caused by the varying overlaps of wave functions for different numbers of electrons.

We have studied how temperature affects Fano resonances. In Fig. 3(a) the resonances are shown for temperatures from $T = 70$ mK to $T = 1$ K. Although the resonance amplitude decreases with increasing temperature, the lineshape described by q clearly remains unaffected. One of the resonances from Fig. 3(a) is analyzed more closely in Fig. 3(b)–(e) in much the same way as in Fig. 2. We have fit the resonance with eq. 2 and found q to be independent of temperature up to 0.4 K (Fig. 3(c)). This is understood in the two-channel model where the non-resonant channel is temperature independent. The resonant channel has all properties of Coulomb blockade including temperature dependence which is due to the Fermi-Dirac broadening of the electrons in the emitter [2]. However, the relative transmission amplitudes and, most important, the phase evolution of both transmission channels remain unaffected. This is why the shape of the

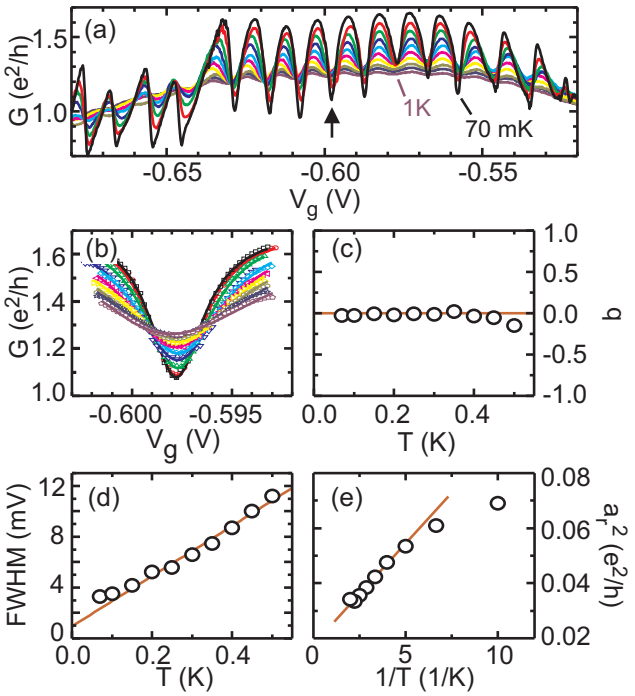

FIG. 3: Fano resonances in the linear conductance for temperatures between $T = 70$ mK (black) and $T = 1$ K (violet). (b) Single Fano anti-resonance marked in (a) for temperatures $T = 70$ mK – 1 K fitted by eq. 2. The temperature dependence of this resonance is further investigated under the following aspects: (c) Asymmetry parameter q, (d) full width at half minimum (FWHM), and (e) transmission a_r^2 of the resonant channel. The temperature scale in (e) is reciprocal.

resonances and q are constant. Only width and amplitude are influenced by the temperature as determined by the emitter.

To further verify the two-channel model we analyze the width Γ of the Fano resonances which is contained in $\tilde{\varepsilon} = (\varepsilon - \varepsilon_0)/(\hbar\Gamma/2)$ in eq. 2. Fig. 3(d) shows that Γ increases linear with temperature. As the non-resonant channel is T-independent, the broadening of the Fano interference directly reflects a broadening of the Coulomb channel. In Coulomb blockade, the slope of $\Gamma(T)$ is $3.5k_BT$ due to Fermi broadening of the emitter [2]. Thus from the slope in Fig. 3(d) we can extract a conversion factor $\alpha = 0.015$ between plunger gate voltage and chemical potential, $\mu = \alpha e V_g$. This has to be compared to $\alpha = 0.045$ from the Coulomb regime at $V_g = -1.15$ V. The difference is attributed to the increased source and drain capacitances at the larger tunnel coupling in the Fano regime.

In Fig. 3(e), the amplitude of the resonant channel a_r^2 is analyzed as a function of temperature. On a reciprocal scale, the amplitude of the resonant channel decreases linearly with increasing temperature as known from Coulomb blockade [2]. Deviations are from thermal decoupling of the electron system from the bath for low temperatures. Please note that as we examine Fano dips originating from destructive interference, a decrease in amplitude in the resonant channel results in an increased total conductance as observed in Fig. 3(b). This mecha-

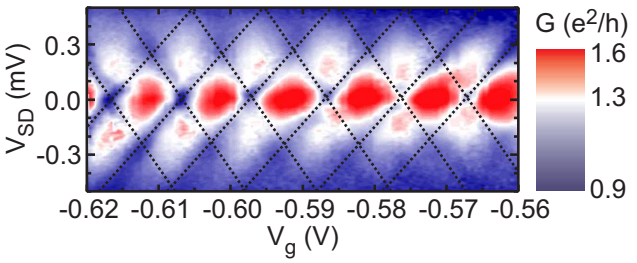

FIG. 4: Nonlinear differential conductance as a function of plunger gate voltage V_g and bias voltage V_{SD} in the $q = 0$ regime of Fano anti-resonances. The diamonds of low conductance known from Coulomb blockade have been replaced by anti-diamonds of high conductance. These are highlighted by black dotted lines.

nism is quite different from the logarithmic temperature dependence of Kondo valleys [3] which might look similar.

At temperatures higher than 0.4 K the overlap of the Fano resonances becomes so strong that our analysis becomes unreliable. It is then impossible to determine the width or amplitude of individual peaks.

The temperature dependence of Fano resonances thus is completely understood in terms of the two-channel model. It results from the Fermi-Dirac broadening of the emitter and its influence on the transmission amplitude and width of the resonant channel. Apparently Fermi-Dirac broadening of the emitter does not influence the non-resonant channel. Our results show that decoherence between both channels can be neglected in our Fano system in the investigated temperature range. Decoherence between both channels would result in a breakdown of the interference. The resonances would then consist of the well-known resonant Coulomb peaks plus an offset from the non-resonant background. Kobayashi and coworkers observed an evolution of Fano resonances to Coulomb peaks plus background at $T \sim 200$ mK in their Aharonov-Bohm ring with an embedded quantum dot [11]. We attribute the strong influence of decoherence in their Fano system to the large size of their system (circumference ~ 4 μm).

Coherence can also be destroyed by finite source-drain voltages. For finite bias voltages quantum dots show so-called Coulomb diamonds in non-linear differential conductance measurements versus source-drain voltage V_{SD} and gate voltage V_g. These are diamond-shaped areas of low conductance. In our Fano quantum dot, however, we observe clear anti-diamonds of *high* conductance for the $q = 0$ regime (Fig. 4). These are again understood in the two-channel model. The resonant channel based on Coulomb blockade determines the resonance positions. The total conductance, however, is determined by the interference of both conductance channels, which leads to anti-diamonds in the $q = 0$ anti-resonance regime. Thus the appearance of anti-diamonds confirms our interpretation of the Fano regime. Non-linear differential conductance measurements also address decoherence. From Fig. 4 it is clear that at least for $V_{SD} = -0.3$ – 0.3 mV the interference is preseved. The decoherence introduced by the finite source-drain voltage V_{SD} is not sufficient to destroy the interference. Finally, Fig. 4 demonstrates the low charging energy in the Fano regime of $U \sim 0.3$ eV. Insertion into the Heisenberg uncertainty relation yields roughly $\Delta t \cdot U \sim 0.1h$. This is consistent with the existence of a direct, virtual, and non-resonant transmission path not respecting Coulomb blockade.

In conclusion, we explored the semi-open Fano regime of quantum dots. We found stable series of resonances with similar lineshapes. We have interpreted our measurements in terms of two interfering transmission channel and extracted phase information for the non-resonant channel. The sudden changes in lineshape were interpreted as charge reconfigurations on the dot influencing the direct non-resonant trajectory. We found our Fano interferometer robust with respect to decoherence in temperature and source-drain voltage dependent measurements.

We thank F. Hohls and U. Zeitler for help with the measurement setup and acknowledge financial support by BMBF.

* Electronic address: fuehner@nano.uni-hannover.de

[1] L. P. Kouwenhoven *et al.*, in *Mesoscopic Electron Transport*, ed. L. L. Sohn *et al.*, (Kluwer, Series E 345, 1997).
[2] C. W. J. Beenakker, Phys. Rev. B **44**, 1646 (1991).
[3] D. Goldhaber-Gordon *et al.*, Nature **391**, 156 (1998); S. M. Cronenwett *et al.*, Science **281**, 540 (1998); J. Schmid *et al.*, Physica B **256**, 182 (1998).
[4] J. P. Bird *et al.*, Rep. Progr. Phys. **66**, 583 (2003).
[5] U. Fano, Phys. Rev. **124**, 1866 (1961).
[6] R. K. Adair *et al.*, **76**, 308 (1949); J. A. Simpson and U. Fano, Phys. Rev. Lett. **11**, 158 (1963).
[7] U. Fano and J. W. Cooper, Phys. Rev. **137**, A1364 (1965).
[8] J. Kim *et al.*, Phys. Rev. Lett. **90**, 166403 (2003).
[9] V. Madhavan *et al.*, Science **280**, 567 (1998); J. Li *et al.*, Phys. Rev. Lett. **80**, 2893 (1998); O. Újsághy *et al.*, Phys. Rev. Lett. **85**, 2557 (2000).
[10] J. U. Nöckel and A. D. Stone, Phys. Rev. B **50**, 17415 (1994).
[11] K. Kobayashi *et al.*, Phys. Rev. Lett. **88**, 256806 (2002).
[12] J. Göres *et al.*, Phys. Rev. B **62**, 2188 (2000).
[13] I. G. Zacharia *et al.*, Phys. Rev. B **64**, 155311 (2001).
[14] S.-J. Xiong and Y. Yin, Phys. Rev. B **66**, 153315 (2002).
[15] E. R. Racec and U. Wulf, Phys. Rev. B **64**, 115318 (2001).
[16] B. R. Bułka and P. Stefański, Phys. Rev. Lett. **86**, 5128 (2001).
[17] W. Hofstetter, J. König, and H. Schoeller, Phys. Rev. Lett. **87**, 156803 (2001).
[18] A. A. Clerk, X. Waintal, and P. W. Brouwer, Phys. Rev. Lett. **86**, 4636 (2001).
[19] A. A. Clerk, P. W. Brouwer, and V. Ambegaokar, Phys. Rev. Lett. **87**, 186801 (2001).
[20] S. Lindemann *et al.*, Phys. Rev. B **66**, 161312 (2002).
[21] R. Schuster *et al.*, Nature (London) **385**, 417 (1997).